Supramolecular self-assembly of DNA with a cationic polythiophene -From polyplexes to fibers

Maxime Leclercq, Jenifer Rubio Magnieto, Danahe Mohammed, Sylvain Gabriele, L Leclercq, Herve Cottet, Sebastien Richeter, Sebastien Clement, Mathieu Surin

Supramolecular self-assembly of DNA with a cationic polythiophene – From polyplexes to fibers

Maxime Leclercq, [a] Jenifer Rubio-Magnieto, [a]† Danahe Mohammed,[b] Sylvain Gabriele, [b] Laurent Leclercq, [c] Hervé Cottet, *[c] Sébastien Richeter, [d] Sébastien Clément,*[d] and Mathieu Surin* [a]

Abstract: Cationic polythiophenes constitute an interesting class of polymers for prospective applications in imaging, gene delivery and biosensing, as they combine solubility in aqueous media and have sensitive optical properties for the detection of biomolecules such as DNA. Here, we study the supramolecular self-assembly of poly[3-(6'-(trimethylphosphonium)hexyl)thiophene-2,5-diyl] (**P3HT-PMe$_3$**) with different types of DNA, such as single-stranded oligonucleotides or long genomic DNA. Self-assembly in buffered aqueous solution yields polyplexes (polymer/DNA complexes) with hydrodynamic radius ranging from 7 nm to around 25 nm, as observed by Taylor Dispersion Analysis. In these polyplexes, the achiral polymer presents chiroptical signals induced by supramolecular organization along chiral DNA. When the solution of long DNA/**P3HT-PMe$_3$** is deposited on surfaces, tens of µm-long fibers are formed by condensation of DNA and compaction of the polyplexes, as evidenced by microscopy techniques.

Supramolecular self-assembly has been thoroughly exploited to achieve well-defined nanostructures for prospective applications in biomedical fields, for instance in regenerative medicine, biosensing, and medical imaging.[1] Fine control over the interactions between biomolecules and synthetic (macro)molecules enable the self-assembly of functional hybrid materials, often referred to as biohybrid materials.[2] Notably, hybrid supramolecular nanostructures combining DNA and synthetic polymers are of high current interest for developing a wide range of applications, notably in gene delivery, sensing, and hydrogels.[3] In this frame, there has been many studies on the design of cationic π-conjugated oligomers or polymers that interact with DNA mainly *via* electrostatic interactions, with applications in the fields of DNA concentration assays and DNA hybridization detection.[4] In this frame, cationic polythiophenes (CPTs) are an interesting class of π-conjugated nanomaterials for binding DNA.[4c, 5] Recently, CPTs were successfully used for DNA delivery into tumour cells,[6] or for the regulation of gene expression through a photoinduced unwinding of plasmid DNA when it is assembled to the CPT.[7] In this context, some of us designed poly[3-(6'-(trimethylphosphonium)hexyl)thiophene-2,5-diyl][8] (**P3HT-PMe$_3$**, see Scheme 1) that showed DNA sequence-dependent chiroptical signals in the spectral range of the polythiophene when mixed with oligonucleotides (ODNs) in solution.[9] Together with the fluorescence of the polymer, the (chir)optical signals were exploited to probe the hybridization between complementary oligonucleotides.[10]

Here, we report on the supramolecular structures formed by the complexation of **P3HT-PMe$_3$** and DNAs of various lengths. We demonstrate that, in aqueous buffered solutions, the self-assembly of **P3HT-PMe$_3$** and DNA leads to the formation of polyplexes (*i.e.* polymer/DNA complexes) with sizes in the range from a few nm for the shortest DNA to around 25 nm for long DNA, which is typically the range for polyplexes currently used for cell transfection.[11] We describe the evolution of the chiroptical properties going from solution to the solid-state, together with a morphological study on the hierarchical self-assembly of long DNA with **P3HT-PMe$_3$** into fiber-like structures extending from µm to hundreds µm in length.

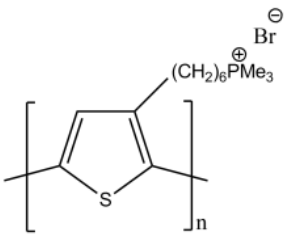

P3HT-PMe$_3$

Scheme 1. Chemical Structure of the cationic poly[3-(6'-(trimethylphosphonium)hexyl)thiophene-2,5-diyl], **P3HT-PMe$_3$.**

[a] M. Leclercq, Dr. J. Rubio-Magnieto, Prof. M. Surin
Laboratory for Chemistry of Novel Materials
Center for Innovation in Materials and Polymers
University of Mons - UMONS, 20 Place du Parc, B-7000 Mons, Belgium. E-mail: mathieu.surin@umons.ac.be

[b] Dr. D. Mohammed, Prof. S. Gabriele
Mechanobiology & Soft Matter Group
Laboratoire Interfaces et Fluides Complexes
Center for Innovation in Materials and Polymers
University of Mons - UMONS, 20 Place du Parc, B-7000 Mons, Belgium.

[c] Dr. L. Leclercq, Prof. H. Cottet
Institut des Biomolécules Max Mousseron (IBMM), Université de

Taylor Dispersion Analysis

Taylor dispersion analysis (TDA) is an absolute method (no calibration required) giving access to diffusion coefficient (or hydrodynamic radius) of any solute in the range of angström up to sub-micron.[12] TDA is based on the analysis of band broadening under a laminar Poiseuille flow in an open tube. In the case of polycation mixtures, TDA give access to the weight-average hydrodynamic radius (R_h).[13] The polyplex, and to the free polycation concentration at equilibrium in the mixture.[14] Figure 1 displays the taylorgram obtained for salmon DNA (**sDNA**) and P3HT-PMe3 polyplex (N/P=12 molar ratio) in frontal mode (continuous injection of the equilibrated mixture in the capillary). The taylorgram is the combination of two *erf* contributions (see experimental part): one pertaining to the free polycation in solution, and the other belonging to the polyplex. By fitting the taylorgram (see experimental part), the R_h of the free polycation chain was determined as 1.4 nm which is, of course, much smaller than the polyplex (25.5 nm). Interestingly, the free polycation concentration at equilibrium in the mixture allows determining the average number of polycation chains per DNA chain $\bar{n}$ = 341 corresponding to a positive to negative charge ratio of n^+/n^- =5.3, which means that the polyplex is highly positively charged. This finding is in agreement with the general rule recently enounced about the overall charge of polyelectrolyte complexes[15] stating that if the polyelectrolyte of highest charge density between the two partners is introduced in excess in the mixture, the complex should have the same charge as this polyelectrolyte (here the polycation). Reversely, if the polyelectrolyte of highest charge density is introduced in default in the mixture, the complex should be stoichiometric (neutral, *i.e.* n^+/n^- =1). Taylorgrams obtained for dT_{20}/P3HT-PMe_3 mixtures at different N/P ratios (1 and 10) are provided in SI. The polyplex size for this system is about 7.3 nm for both N/P ratio. As expected from the rule previously enounced, the polyplex charge is stoichiometric in the case of N/P=1 ratio, and highly positively charged (n^+/n^- =5) for the N/P=10 (see Table 1).

Table 1. Polyplex average hydrodynamic radii (R_h), average number of ligands per DNA chain $\bar{n}$ and charge ratio stoichiometry n^+/n^- in the polyplex obtained by TDA for the different systems based on P3HT-PMe_3 polycation.

Polyplex (ODN/ P3HT-PMe_3)	N/P ratio	R_h (nm)	% of free P3HT-PMe_3	$\bar{n}$	n^+/n^-
sDNA/P3HT-PMe_3	12	25.5 ±1.8	56 ±1	341	5.3
dT_{20}/P3HT-PMe_3	1	7.2 ±0.6	4 ±1	0.3	1.0

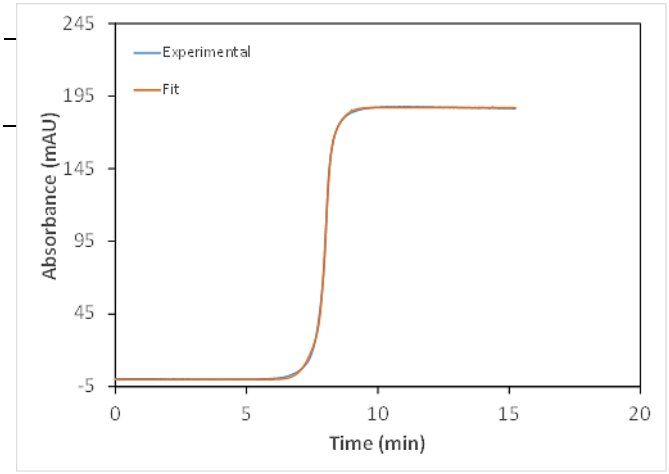

Figure 1. Taylorgram obtained for sDNA/P3HT-PMe_3 polyplex (N/P=12) in frontal mode. Experimental conditions: PDADMAC-coated capillary 40 cm total length (30 cm to the UV detector) × 50 µm i.d. Eluent: TE buffer. Mobilization pressure: 30 mbar. UV detection: 214 nm. Temperature: 25 °C. Erf fitting is displayed in red; experimental data are in blue.

Chiroptical properties of polyplexes

UV-Vis absorption and Circular Dichroism (CD) spectroscopies were carried out on aqueous mixtures of **P3HT-PMe_3** and DNA in various proportions in the same solution conditions than TDA studies (in TE buffer at pH 7.4). A large red-shift of the UV-Vis maximum absorption wavelength is observed when the polymer is mixed with oligonucleotide **dT_{20}** ($\Delta\lambda_{max}$ = +25 nm at 1:1 ratio). Figure 2a shows the CD spectra of **dT_{20}/P3HT-PMe_3** at a 1:1 charge ratio. Compared to the CD spectra of the pure compounds in the same conditions, two important effects are observed: (i) a decrease of CD signal in the wavelength range from 230-300 nm with respect to the pure DNA, and (ii) the appearance of a bisignate (+/-) induced CD signal (ICD) in the spectral range of **P3HT-PMe_3** (from 400 nm to 600 nm). This ICD signal is the signature of a right-handed helical

conformation/aggregation of the polymer chain in the DNA/polymer complex.

When a long DNA (salmon DNA, **sDNA)** was mixed with **P3HT-PMe$_3$** at a 1:1 charge ratio in aqueous buffered solution, the red-shift of the polymer main absorption band is also observed ($\Delta\lambda_{max}$ = +6 nm, see **ESI**), but much weaker than for mixtures with single-stranded DNAs (for example, with **dT20,** $\Delta\lambda_{max}$ is +25 nm). The CD signal in the range 230-300 nm slightly decreased and we did not observe any ICD signal in the range 400-600 nm (Figure 1b). However, when the charge ratio is higher, a weak ICD signal is observed (see ESI), but much weaker than the ICD signals observed in mixtures with single-stranded oligonucleotides. The differences in the UV-Vis and CD spectra for mixtures with short oligonucleotides and long double-stranded DNA (salmon DNA) likely arises in the binding mechanisms: with single-stranded DNAs, besides electrostatic interactions, monomer-nucleobase interactions can occur (notably π-type interactions), which planarize the π-conjugated backbone. In contrast, with double-stranded DNAs the bases are paired in the inner part of DNA, and thus the monomer-nucleobase interactions are less likely. [10]

The CD spectra of **sDNA/P3HT-PMe$_3$** complex was measured in thin films deposited on quartz substrates, see Figure 2b (orange line). The CD spectrum is remarkably different than in solution: i) a CD signal is observed in the visible range, where only the polymer absorbs, and ii) in the range 230-300 nm, the CD signals (negative peak at 300 nm and a positive peak at 230 nm) are inverted compared to both pure **sDNA** and **sDNA/P3HT-PMe$_3$** mixture in solution. This reversed CD signal is the signature of a condensed and compacted DNA, as observed in so-called Polymer-Salt-Induced (PSI) aggregates.[16]

Microscopic morphology of polyplexes on surfaces

To further investigate possible hierarchical self-assembly processes of the polyplexes on surfaces, we studied thin deposits of the mixture solution by microscopy techniques. Figure 3 shows Atomic Force Microscopy (AFM) images of thin deposits (made by soaking the mica substrate into solutions) of pure **P3HT-PMe$_3$** (Fig. 3a), pure **sDNA** (Fig. 3b), and **sDNA/p3HT-PMe$_3$** (Fig. 3c-d) on a mica substrate (dry thin deposits). Figure 3a showed that the pure polymer forms granular structures of varying sizes, with an average width of around 0.1 µm and an average thickness of 1.7 nm. Thin deposits of pure **sDNA** showed the typical worm-like structures of DNA (Fig. 3b). In contrast to the morphologies of pure compounds, thin deposits of **sDNA/P3HT-PMe$_3$** exhibit a dendritic morphology (Fig. 3c), *i.e.* tens of µm-long elongated aggregates with fiber-like branches (see zoom in Fig. 3d) that extend over a few µm. In Fig. 3c, the width and thickness of the main stem appearing in diagonal of the image are above 1 µm and around 8 nm, respectively. The branches at the periphery of this structure have a diameter ranging from 0.1 µm to 0.25 µm, and a thickness of 3 nm in average. The granular structures present in between the dendrites (or branches) are reminding the morphology of the pure polymer (see Fig. 3a). Hence, the self-assembly of **sDNA** with **P3HT-PMe$_3$** leads to an extended dendritic morphology with different levels of organization. These observations can be related to the works of Knaapila, Scherf, *et al.*, who studied the self-assembly of salmon DNA with a π-conjugated copolymer containing a cationic polythiophene block, at various charge ratios.[17] They showed that the self-assembly between the copolymer and DNA can yield fractal sub-micrometer-scaled structures, such as the dendritic morphology observed here. Note that the sharpest fibers on the Fig.3d have an average diameter around 30.0 nm ± 3 nm. This is to compare to the estimates of the R_h of around 25 nm in solution. It is likely that the fibers grow by compaction and coalescence of polyplexes along an axis during the deposit formation.

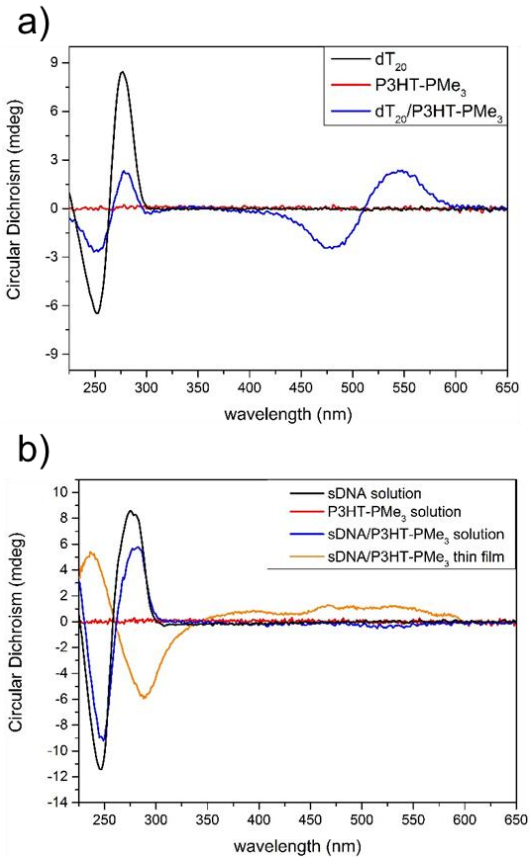

at their periphery.

Figure 2. a) CD spectra of $\mathbf{dT_{20}}$ (black line), $\mathbf{P3HT\text{-}PMe_3}$ (red line) and $\mathbf{dT_{20}/P3HT\text{-}PMe_3}$ complex (blue line) at a 1:1 DNA/polymer charge ratio; b) CD spectra of **sDNA** (black line), $\mathbf{P3HT\text{-}PMe_3}$ (red line), and $\mathbf{sDNA/P3HT\text{-}PMe_3}$ complex (blue line) in solutions at a 1:1 DNA/polymer charge ratio; the solid state CD spectrum of thin films of $\mathbf{sDNA/P3HT\text{-}PMe_3}$ **(**charge ratio 1:3) is shown (orange line).

Confocal Optical Microscopy (COM) was used to visualise the $\mathbf{sDNA/P3HT\text{-}PMe_3}$ complexes at a larger scale and to observe the fluorescence of the complexes when the samples are excited at 480 nm. Note that here the samples are studied at the interface solution/surface, from a droplet deposited on a glass substrate. Figure 4a shows a large-scale image with many coiled fiber-like structures of different sizes (typically a few tens µm-long), which are reminiscent of the elongated µm-wide fiber-like aggregates observed with AFM. Since those fibers were observed in both types of AFM and COM analyses, this means that the self-assembly into fibers occurs at the solution/surface interface. A zoom showing the fluorescence image (excitation at 480 nm) of a particularly long fiber is shown in Fig. 4b, where we can observe the dendritic structure as observed with AFM. Strikingly, a relatively homogeneous fluorescence is observed on both the large fiber and smaller branches, which shows that the polymer is homogeneously complexed within the fibers. Based on the length distribution of the fibers (shown in Fig. 4c for a population over a hundred fibers), we estimated the median being at 21 µm.

Both microscopy analyses showed us the evolution of the morphology going from the pure compounds to the morphology arising from the self-assembly of **sDNA**/ $\mathbf{P3HT\text{-}PMe_3}$, for which a dendritic structure is observed with large fibers extending over tens of µm and thinner branched nanostructures

[Tapez ici]

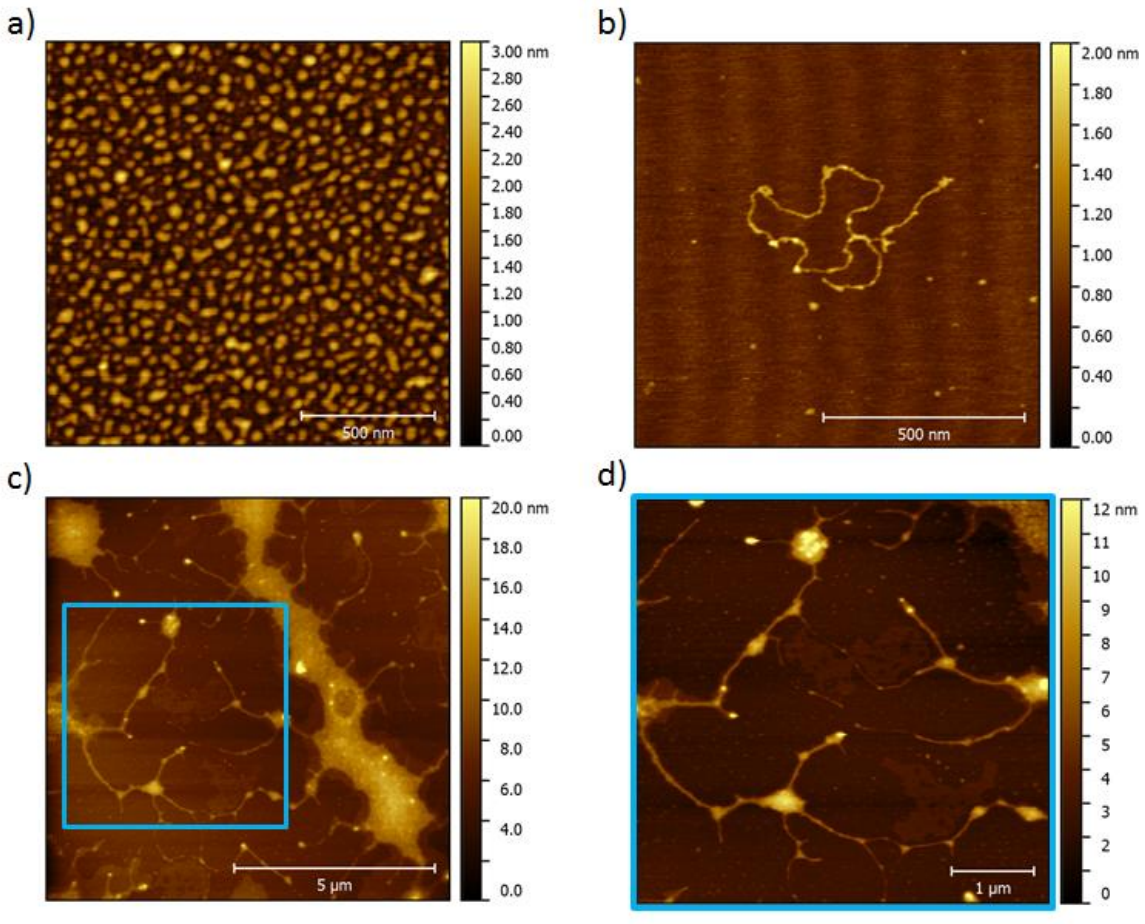

Figure 3. Tapping-Mode AFM images of thin deposits on mica of solutions of: a) pure **P3HT-PMe$_3$**; b) pure **sDNA**, and (c,d) **sDNA/P3HT-PMe$_3$** complexes. Image in d) corresponds to a zoom in the area marked by a blue square depicted in c).

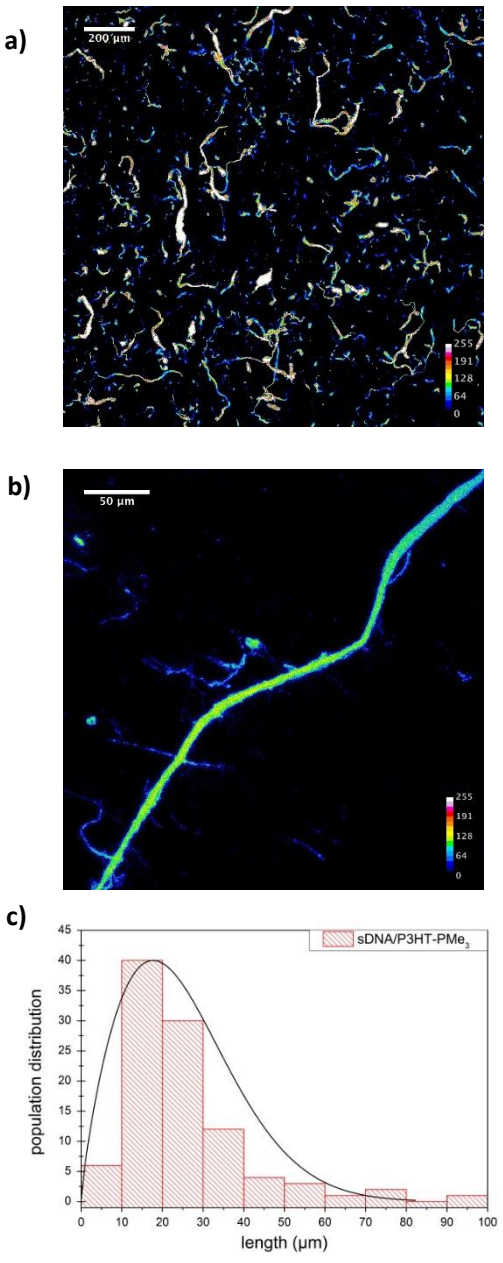

Figure 4. a) (1640 µm)², and b) (320 µm)² confocal optical microscopy images of **sDNA/P3HT-PMe$_3$** with the fluorescence intensity (colour scale). (c) size distribution of the fibers along their long axis. The excitation wavelength was 480 nm to show the fiber fluorescence. The concentration of **sDNA** is 0.12 µM and the concentration of polymer is 5 µM.

Altogether, these results bring new insights into the self-assembly of DNA with cationic polythiophenes in aqueous solution and on surfaces. The size of the polyplexes in solution are of a few nm in case of assemblies with short single-stranded DNA. For long DNA (thousands base pairs), the size of the complex typically ranges in the application as polyplexes, with a R_h of around 25 nm for a *N/P* ratio of 12. When the solution is deposited on a surface, we observed the formation of dendritic fibers, that can extend over tens of µm. Along these fibers, the π-conjugated polymer shows a homogeneous luminescence, and the DNA is likely compacted in psi-aggregate, as indicated by CD in the solid-state. Altogether, these results provide some guidelines towards the formation of DNA/CPT assemblies as polyplexes for prospective applications in cell transfection, or self-assembled fibers for organic bioelectronics.

Experimental Details

P3HT-PMe$_3$ (average molecular weight M_n ~ 17,686 g.mol^{-1}) was synthesized as reported earlier[8,9] and dissolved in TE buffer (10 mM of Tris-HCl and 1 mM of EDTA). Salmon DNA samples were purchased from Aldrich and oligonucleotides were purchased from Eurogentec (Belgium) with the highest purity grade (> 95% pure in sequence) in the dried state. DNA samples were dissolved in a volume of TE buffer (pH 7.4, 10 mM Tris buffer and 1mM EDTA) at stock concentration of 170 µM for **dT$_{20}$** and 0.6 µM (in strands) for **sDNA** of 170 µM. ODN solutions were centrifuged during 2 minutes at 2000 rpm. Typically, volumes of 20 µL of this solution were used to prepare different aliquots, to which were added TE buffer, and the final solution was mixed using a vortex. The exact concentration of DNA in the buffer solution was determined by UV-Vis absorption at 25 ºC using the specific extinction coefficients at 260 nm (ε_{260}): 162600 L.mol^{-1}.cm^{-1} for **dT$_{20}$** and 13200 L.mol^{-1}.cm^{-1} by base pairs (bp) for **sDNA**. The formation of **DNA/ P3HT-PMe$_3$** complexes was studied in TE buffer, mixing the **P3HT-PMe$_3$** with each different DNA sample at vigorous speed for 1 minute and allowed to equilibrate for at least 10-15 minutes.

Spectroscopy. UV-Vis absorption and CD measurements were recorded using a Chirascan^{TM} Plus CD Spectrometer from Applied Photophysics. The measurements were carried out using 2 mm suprasil quartz cells from Hellma Analytics. The spectra were recorded between 230 and 650 nm, with a bandwidth of 1 nm, time per point 0.5 s and two repetitions. The buffered water solvent reference spectra were used as baselines and were automatically subtracted from the CD spectra of the samples. For the CD spectra in solid state, a droplet of solution was deposited on a quartz suprasil plate and we let the sample dry. The solid-state study was carried out using a Chirascan CD integrating sphere with a high diffuse reflection factor, increasing the number of light beams to the CD detector. For microscopy studies, the sample solutions were the same as for spectroscopic studies.

Microscopy. Samples for AFM imaging were produced as follows: freshly-cleaved mica substrates were used and sunk into the solution during 5 to 10 min. The samples were then removed from the solution and washed with Milli-Q water, and then dried with a gentle nitrogen flow. The AFM analyses were carried out in Tapping-Mode in air at room temperature using a Nanoscope III from Bruker, using NCHV tips (f_0 = 320 KHz) from Bruker probes. Confocal optical microscopy images were carried out by placing droplets of solutions images were taken with a 1024x1024 pixels resolution (length and width images = 1640 µm).

Formation of polyplexes. Polyplexes were prepared directly before TDA experiments. A 0.116 g/L double-stranded salmon DNA (sDNA) solution and a 4.5 g/L P3HT-PMe$_3$ polycation solution were prepared in TE buffer (10 mM TRIS-HCl, 1 mM EDTA at pH 7.4). A 30 µL aliquot of P3HT-PMe$_3$ solution was first added to 70 µL TE buffer solution. The resulting mixture was then added to a 100 µL sDNA solution and shortly stirred at room temperature. N/P molar ratio was 12. Similar procedure was applied to the oligonucleotides dT$_{20}$. A 0.85 g/L oligonucleotide solution and a 45 g/L P3HT-PMe$_3$ polycation solution were prepared in TE buffer. A 5 µL aliquot of P3HT-PMe$_3$ solution was added to a mixture composed of 250 µL dT$_{20}$ solution and 45 µL TE buffer solution. N/P molar ratio was 1. A 50 µL aliquot of P3HT-PMe$_3$ solution was added to a 250 µL dT$_{20}$ solution. N/P molar ratio was 10. The resulting mixtures were

shortly stirred at room temperature. In all cases, polyplexes were allowed to equilibrate for 30 min before analysis by TDA.

Taylor Dispersion Analysis experiments (TDA). Capillaries were prepared from bare silica tubing purchased from Polymicro Technologies (Photon Lines, Saint-Germain-en-Lay, France). All TDA experiments were carried out at 25°C using frontal mode (i.e. by continuous injection of the sample). Each sample is prepared in the background electrolyte (TE buffer: 10 mM TRIS-HCl, 1 mM EDTA, pH 7.4). Before sample analysis, the capillary was previously filled with the same buffer. All TDA experiments were realized in triplicates.

TDA experiments were performed on a P/ACE MDQ system (Beckman, USA) using 50 µm i.d. × 40 cm (30 cm to the detector) capillaries. Capillaries were coated with poly(diallyl dimethyl ammonium chloride) (PDADMAC, M_w = 500,000 g/mol). For that, the capillaries were first conditioned with 1 M NaOH for 20 min and water for 5 min, then flushed with a 0.2 % PDADMAC aqueous solution for 10 min, and finally flushed with TE buffer for 10 min. TDA experiments were carried out using 30 mbar mobilization pressure. Solutes were monitored by UV absorbance at 214 nm.

To increase the detection sensitivity, TDA was implemented in frontal mode, meaning that the sample is continuously and hydrodynamically injected into the capillary [13], leading to the detection of a front instead of a peak. For a bimodal mixture composed of two populations of different sizes, the temporal signal front is given by:

$$S(t) = \frac{S_1+S_2}{2} + \frac{S_1}{2}\mathrm{erf}\left(\frac{t-t_0}{\sigma_1\sqrt{2}}\right) + \frac{S_2}{2}erf\left(\frac{t-t_0}{\sigma_2\sqrt{2}}\right) \quad (1)$$

where t_0 is the average elution time, σ_1 and σ_2 are the square roots of the temporal variance of the two contributions in the elution profile, and S_1 and S_2 are two constants that depend on the response factor and injected quantity of the two populations present in the solute.

Equation (1) is valid provided that t_0 is much longer than the characteristic diffusion time of the solute in the cross section of the capillary ($t_0 \geq 1.25R_c^2/D$ for a relative error ε on the determination of D lower than 3%) and that the axial diffusion is negligible compared to convection (the Peclet number $P_e = R_c u / D$ is above 40 for ε lower than 3%, with u being the average linear mobile phase velocity)[18]

The hydrodynamic radii R_h of the two species are related to their corresponding σ^2 according to:

$$R_h = \frac{k_B T}{6\pi\eta D} = \frac{4\sigma^2 k_B T}{\pi\eta R_c^2 t_0} \quad (2)$$

where k_B is the Boltzmann constant, T is the temperature (in K), R_c is the capillary diameter, and η is the viscosity of the eluent (0.9×10^{-3} Pa.s for TE buffer).

In this work, DNA (sDNA or dT_{20}) and P3HT-PMe_3 polycation were considered as substrate (S) and ligand (L), respectively. Polyplex $SL_{\bar{n}}$ are composed of one substrate S and $\bar{n}$ ligands (L), where $\bar{n}$ is the stoichiometry of the polyplex which is given by:

$$\bar{n} = \frac{[L]_0-[L]}{[S]_0} \quad (3)$$

where $[L]_0$ and $[S]_0$ are the initial introduced concentrations of the ligand and the substrate, respectively, and $[L]$ is the free polycation (ligand) concentration. $[L]$ is obtained from the signal contribution due to the free ligand by external calibration (see SI for the calibration curve).

Acknowledgements

This work was supported by the Fonds de la Recherche Scientifique-FNRS (Belgium) under the grants n°1.B333.15F (CHIRNATES) and n°F.4532.16 (MIS-SHERPA). J.R.-M. and M.S. are FNRS researchers. The authors also thank CNRS and the Université Montpellier for financial support.

Keywords: supramolecular self-assembly • DNA • cationic polythiophene • polyplexes • fibers

[1] a) E. Busseron, Y. Ruff, E. Moulin, N. Giuseppone, *Nanoscale* **2013**, *5*, 7098-7140; b) *Supramolecular Systems in Biomedical Fields,* Ed. H.-J. Schneider, RSC Publishing, Cambridge, **2013**; c) J. Boekhoven, S. I. Stupp, *Adv Mater* **2014**, *26*, 1642-1659; d) M. Kumar, P. Brocorens, C. Tonnelé, D. Beljonne, M. Surin, S. J. George, *Nat Commun* **2014**, *5*, 5793; e) M. Palma, J. G. Hardy, G. Tadayyon, M. Farsari, S. J. Wind, M. J. Biggs, *Adv Healthc Mater* **2015**, *4*, 2500-2519.

[2] a) Y. Ruff, T. Moyer, C. J. Newcomb, B. Demeler, S. I. Stupp, *J Am Chem Soc* **2013**, *135*, 6211-6219; b) N. Stephanopoulos, R. Freeman, H. A. North, S. Sur, S. J. Jeong, F. Tantakitti, J. A. Kessler, S. I. Stupp, *Nano Lett* **2015**, *15*, 603-609; c) Y. Wang, K. S. Schanze, E. Y. Chi, D. G. Whitten, *Langmuir* **2013**, *29*, 10635-10647; d) S. L. Kuan, Y. Wu, T. Weil, *Macromol Rapid Commun* **2013**, *34*, 380-392; e) R. Freeman, N. Stephanopoulos, Z. Alvarez, J. A. Lewis, S. Sur, C. M. Serrano, J. Boekhoven, S. S. Lee, S. I. Stupp, *Nat Commun* **2017**, *8*, 15982.

[3] a) B. Shi, M. Zheng, W. Tao, R. Chung, D. Jin, D. Ghaffari, O. C. Farokhzad, *Biomacromolecules* **2017**, *18*, 2231-2246; b) H. Tang, X. Duan, X. Feng, L. Liu, S. Wang, Y. Li, D. Zhu, *Chem Commun* **2009**, 641-643; c) C. K. McLaughlin, G. D. Hamblin, H. F. Sleiman, *Chem Soc Rev* **2011**, *40*, 5647-5656.

[4] a) B. S. Gaylord, A. J. Heeger, G. C. Bazan, *J Am Chem Soc* **2003**, *125*, 896-900; b) C. Chi, A. Mikhailovsky, G. C. Bazan, *J. Am. Chem. Soc.* **2007**, *129*, 11134-11145; c) H.-A. Ho, A. Najari, M. Leclerc, *Acc. Chem. Res.* **2008**, *41*, 168-178; d) C. Zhu, L. Liu, Q. Yang, F. Lv, S. Wang, *Chem. Rev.* **2012**, *112*, 4687-4735; e) F. Xia, X. Zuo, R. Yang, Y. Xiao, D. Kang, A. Vallee-Belisle, X. Gong, A. J. Heeger, K. W. Plaxco, *J Am Chem Soc* **2010**, *132*, 1252-1254; f) Z. Liu, H. L. Wang, M. Cotlet, *Chem Commun* **2014**, *50*, 11311-11313.

[5] a) K. P. Nilsson, O. Inganäs, *Nat Mater* **2003**, *2*, 419-424; b) M. Hamedi, A. Elfwing, R. Gabrielsson, O. Inganäs, *Small* **2013**, *9*, 363-368; c) F. Wang, M. Li, B. Wang, J. Zhang, Y. Cheng, L. Liu, F. Lv, S. Wang, *Sci Rep* **2015**, *5*, 7617.

[6] C. Zhang, J. Ji, X. Shi, X. Zheng, X. Wang, F. Feng, *ACS Appl Mater Interfaces* **2018**, *10*, 4519-4529.

[7] G. Yang, H. Yuan, C. Zhu, L. Liu, Q. Yang, F. Lv, S. Wang, *ACS Appl Mater Interfaces* **2012**, *4*, 2334-2337.

[8] S. Clément, A. Tizit, S. Desbief, A. Mehdi, J. De Winter, P. Gerbaux, R. Lazzaroni, B. Boury, *J. Mater. Chem.* **2011**, *21*, 2733-2739

[9] J. Rubio-Magnieto, A. Thomas, S. Richeter, A. Mehdi, P. Dubois, R. Lazzaroni, S. Clément, M. Surin, *Chem. Commun.* **2013**, *49*, 5483-5485.

[10] a) J. Rubio-Magnieto, E. G. Azene, J. Knoops, S. Knippenberg, C. Delcourt, A. Thomas, S. Richeter, A. Mehdi, P. Dubois, R. Lazzaroni, D. Beljonne, S. Clément, M. Surin, *Soft Matter* **2015**, *11*, 6460-6471; b) J. Knoops, J. Rubio-Magnieto, S. Richeter, S. Clément, M. Surin, in *Materials and Energy, Vol. 9* (Ed.: M. Knaapila), World Scientific, **2018**, pp. 139-157.

[11] U. Lächelt, E. Wagner, *Chem Rev* **2015**, *115*, 11043-11078.

[12] H. C. J. Chamieh, *Size-based characterization of nanomaterials by Taylor dispersion analysis, Chapter 9*, Eds. H. Ohshima and K. Makino, Elsevier,Amsterdam (The Netherlands), **2014**.

[13] H. Cottet, J. P. Biron, M. Martin, *Anal Chem* **2007**, *79*, 9066-9073.

[14] S. R. L. Leclercq, J. Chamieh, E. Wagner, H. Cottet, *Macromolecules* **2015**, *48*, 7216-7221.

[15] J. C. F. Lounis, P. Gonzalez, H. Cottet, L. Leclercq, *Macromolecules* **2016**, *49*, 3881-3888.

[16] a) V. A. Bloomfield, *Biopolymers* **1997**, *44*, 269-282; b) B. I. Kankia, V. Buckin, V. A. Bloomfield, *Nucleic Acids Res.* **2001**, *29*, 2795-2801.

[17] M. Knaapila, T. Costa, V. M. Garamus, M. Kraft, M. Drechsler, U. Scherf, H. D. Burrows, *Macromolecules* **2014**, *47*, 4017-4027.

[18] H. Cottet, J. P. Biron, M. Martin, *Analyst* **2014**, *139*, 3552-3562.

SUPPORTING INFORMATION